

Modulation of high quality factors in rolled-up microcavitiesYangfu Fang,¹ Shilong Li,^{2,*} and Yongfeng Mei^{1,†}¹*Department of Materials Science, Fudan University, 220 Handan Road, Shanghai 200433, China*²*National Laboratory for Infrared Physics, Shanghai Institute of Technical Physics, Chinese Academy of Sciences, 500 Yutian Road, Shanghai 200083, China*

(Received 29 June 2016; published 2 September 2016)

We systematically investigate the evolution of resonant modes in a rolled-up microcavity as the overlap length between structural notches increases, which presents a modulation behavior for high Q factors. The resonant modes in the rolled-up microcavity display a deterministic mode chirality, which is well correlated to the Q factor. We derive a two-mode non-Hermitian Hamiltonian to clarify these unusual findings. It reveals that strong resonant interactions of scattered waves between the structural notches are responsible for the high mode chirality (thus high Q factor) and its modulation behavior in rolled-up microcavities.

DOI: [10.1103/PhysRevA.94.033804](https://doi.org/10.1103/PhysRevA.94.033804)**I. INTRODUCTION**

Because of the ultrahigh quality (Q) factor of whispering gallery modes (WGMs), dielectric microcavities with a circular cross section are continuously receiving a great deal of attention over a wide range of applications from cavity quantum electrodynamics to label-free optical biodetection [1–8]. Several geometrical alternatives [9–15], including microspheres, microdisks, microtoroids, microrings, microbotles, microtubes, and microbubbles, have been demonstrated over the last two decades, benefiting from emerging micro- and nanotechniques. By combining top-down (through the design of planar nanomembranes) and bottom-up (through the self-assembly of rolled-up architectures) approaches, rolled-up WGM microcavities have been demonstrated [16–22] and have received much attention owing to the customizability of their geometry and material, as well as their laboratory-on-a-chip compatibility [23]. Recently, nontrivial optical phenomena (i.e., Berry phase and spin-orbit coupling of light) have been observed in WGM microcavities based on the rolled-up geometry [24]. Unfortunately, the Q factor of rolled-up microcavities is undesirably low compared with that of other WGM microcavities. Several loss mechanisms of the Q factor in rolled-up microcavities have been proposed [20], including the material absorption, surface roughness, and the local structural defects (e.g., notches formed by the edges of the rolled-up nanomembrane layer and voids between these layers). Obviously, the usage of these redundant external factors is not helpful to capture the essential physics behind the spoiling of Q factors in rolled-up WGM microcavities.

The ultrahigh Q factor of WGMs is protected by the rotational symmetry of circular microcavities. For a microcavity that has a slight deformation from a circle, the degree of Q spoiling is not severe because of an intrinsic barrier formed by the Kolmogorov-Arnold-Moser (KAM) invariant tori [25]. Rolled-up microcavities are considered as such slightly deformed microcavities. Recently, a nontrivial mechanism of Q spoiling in a slightly deformed microcavity was proposed which points out that Q factors are spoiled

when an $(l, m) = (1, m)$ WGM interacts with its pair $(2, m - 4)$ quasinormal mode through an avoided resonance crossing due to the Fermi resonance [26,27]. Here, l and m are the radial and azimuthal mode indices, respectively. However, the Q -spoiling mechanism due to the Fermi resonance is not applicable for rolled-up microcavities since there is no available $(2, m - 4)$ mode due to their subwavelength-thin wall thickness. Therefore, an in-depth study on the underlying physical mechanism of Q spoiling in rolled-up WGM microcavities is highly required for further development.

Here, we clarify the mechanism of Q spoiling in rolled-up microcavities by systematically investigating the evolution of resonant modes as the overlap length between structural notches increases. The Q factor of resonant modes in a rolled-up microcavity is fully regulated by the deterministic mode chirality. In addition, a modulation behavior of locally high Q factors (thus high mode chiralities) is observed. To explain these unusual findings, a two-mode non-Hermitian Hamiltonian is presented. It reveals that strong resonant interactions of scattered waves between the structural notches through the subwavelength-thin wall result in the high mode chirality (thus high Q factor) and its modulation behavior. These results will help with the understanding and optimization of high- Q rolled-up microcavities as well as other deformed microcavities.

The remainder of this paper is organized as follows. Section II defines the system under study, i.e., rolled-up microcavities. Then, numerical results for their optical resonant modes are presented in Sec. III. In Sec. IV, a non-Hermitian Hamiltonian based on a two-mode approximation is introduced to describe the resonant modes of the rolled-up microcavities. We summarize our results in Sec. V.

II. THE SYSTEM

Figure 1 shows a schematic drawing of a strain-driven self-rolling structure. The resulting rolled-up structure is completely determined by the planar strained dielectric nanomembrane [19,28]. Light confined inside the dielectric wall due to the total internal reflection between the inner and outer surfaces can travel around the circumference leading to WGMs [16]. Dielectric microcavities produced in this way have an excellent customizability of their structural parameter. In this work,

*shilong@mail.sitp.ac.cn

†yfm@fudan.edu.cn

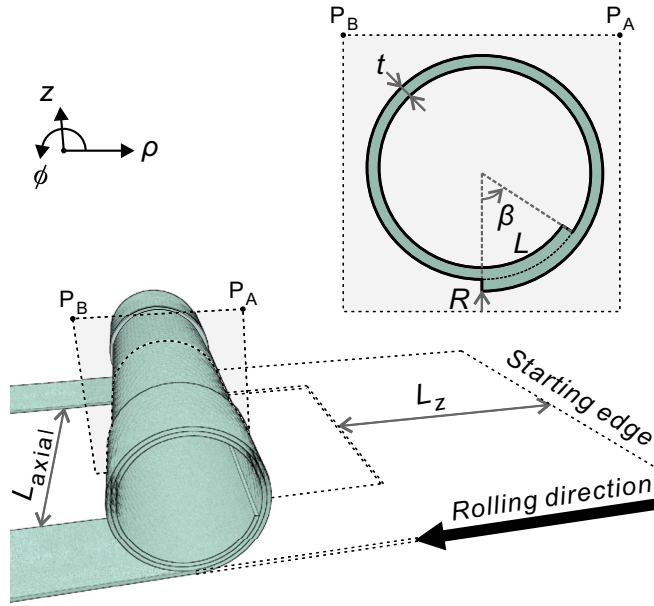


FIG. 1. Schematic of a rolled-up microcavity. A U-shaped strained nanomembrane is defined at the beginning. Then, the self-rolling mechanism starts from the starting edge, and a tubular structure is formed over the full width of the strained nanomembrane. After the rolling distance L_z , only the side pieces of the structure continue to roll. As a result, the middle piece of the structure is separated from the substrate (not shown here) so that scattering loss of resonant modes caused by the substrate is avoided. In the end, a rolled-up microcavity is formed in the middle piece of the self-rolling tubular structure with a well-defined overlap length L , as shown in the inset.

we can thus define the overlap length L as a well-controlled deformation parameter for rolled-up microcavities in order to investigate the evolution of the Q factor of the WGMs.

The axial length L_{axial} (aligned along the z axis) is defined to a very large value (compared to the wavelength considered) so that the rolled-up structure can be treated as an infinitely long cylinder. Maxwell's equations are then reduced to the two-dimensional scalar Helmholtz equation, in polar coordinates (ρ, ϕ) ,

$$\nabla^2 \psi + n^2(\rho, \phi) \frac{\omega^2}{c^2} \psi = 0, \quad (1)$$

where ψ is the wave function, $n(\rho, \phi)$ is the piecewise constant refractive index, ω is the complex frequency, and c is the speed of light in vacuum. Because of the subwavelength-thin wall thickness commonly used in rolled-up microcavities, resonant modes with the transverse magnetic (TM) polarization preferably exist and are considered here. For TM modes, the electric field vector $\mathbf{E}(\rho, \phi, t) \propto (0, 0, \text{Re}[\psi(\rho, \phi)e^{-i\omega t}])$ is along the z direction. The lack of rotational symmetry in rolled-up microcavities makes the optical system nonintegrable, so the finite-element method is adopted to solve the Helmholtz equation (1) with Sommerfeld outgoing wave conditions at infinity [29]. In the end, Q factors are obtained as $|\text{Re}(\omega)/[2\text{Im}(\omega)]|$.

In a given z plane, the boundary of a rolled-up structure is defined as

$$\rho(\phi) = R \left(1 - \frac{t}{2\pi} \phi \right), \quad (2)$$

where R is the outermost radius at $\phi = 0$ and t is the thickness of a single layer. The outer boundary jumps back to R at $\phi = 2\pi$, creating the outer notch, while the inner notch is generated at $\phi = \beta \approx L/R_{\text{avg}}$. Here, the overlap length L is determined by the rolling distance L_z ($L \approx L_z - 2\pi R_{\text{avg}}$), and R_{avg} is the average radius of the rolled-up structure. This spiral-like structure has a deterministic structural chirality, which is counterclockwise (CCW) because the strained nanomembrane is defined to roll upward. The opposite structural chirality (i.e., clockwise, CW) can be obtained by inverting the strain gradient of the strained nanomembrane so that it rolls downward [17]. As will be seen later, this structural chirality determines the spatial chirality of resonant modes in rolled-up microcavities.

A rolled-up microcavity rolled from a 100-nm-thick nanomembrane ($t = 100$ nm), with the refractive index $n = 2$ and the outermost radius $R = 5 \mu\text{m}$, is considered throughout this paper; these are typical parameters for rolled-up microcavities.

III. NUMERICAL RESULTS

Resonant modes in the rolled-up microcavity are presented in Figs. 2(a) and 2(b), which show their wavelength shift and Q -factor variation, respectively. There is a nearly degenerate pair of modes for a given azimuthal mode index m . It is called mode splitting and has recently been proved experimentally [30]. Several numerical studies on the mode splitting have been reported as well [30–32]. It is concluded that the split-mode pairs result from the local structural singularities (i.e., the inner and outer notches), which limit Q factors of rolled-up microcavities. However, none of these works addressed the relationship between Q factors and the structural chirality. The aim of this work is to present a numerical and theoretical study which reveals that Q factors of the split modes are essentially determined by the interplay between the structural and mode chiralities in rolled-up microcavities.

The nearly degenerate mode pairs are well known in the high- Q WGM microcavities (e.g., microspheres [33,34], microdisks [35,36], and microtoroids [6,37]). However, they are generally undesirable due to uncontrollable structure defects which introduce external decay channels, leading to the degradation of the high Q factors [34]. On the other hand, manageable degenerate mode pairs are of particular interest in the context of modern sensing applications [6,38,39]. Recently, Wiersig systematically investigated the structure of nearly degenerate mode pairs in a well-defined two-particle-microdisk system and pointed out that the pair of modes is nonorthogonal and chiral due to an asymmetric transition between the CW and CCW components [40]. A complex-square-root topology with a branch-point singularity at the exceptional point (EP) in parameter space is responsible for the mode chirality and nonorthogonality. Later, he found that the sensitivity of single-particle detection based on the frequency splitting could be enhanced more than threefold

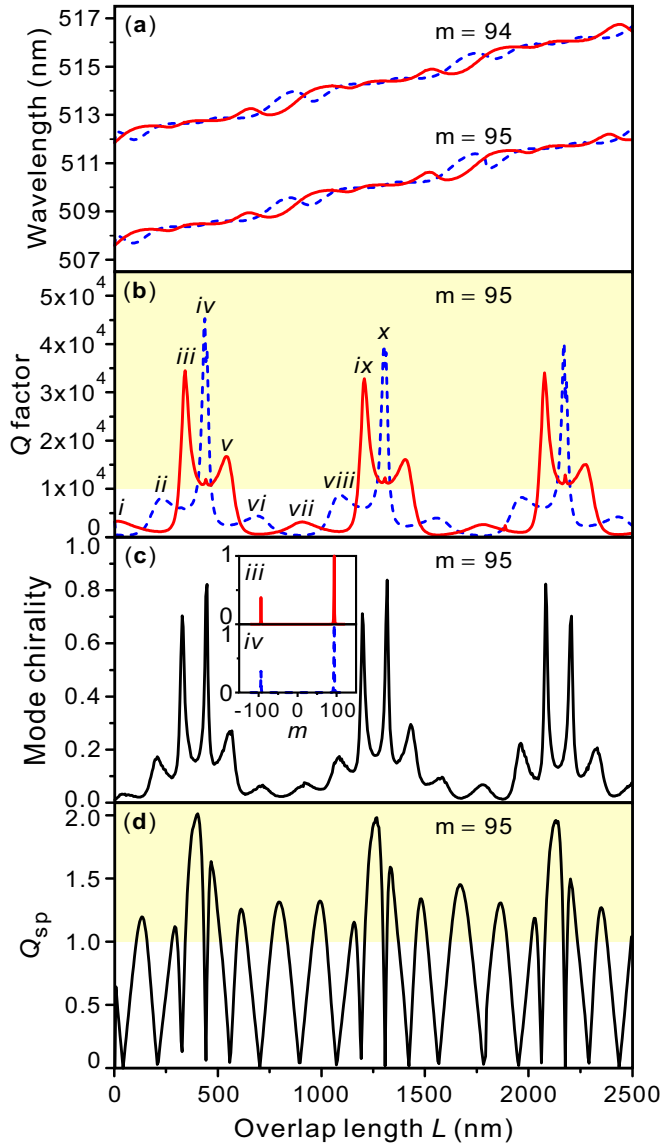


FIG. 2. Evolution of (a) resonant wavelength, (b) Q factor, (c) mode chirality, and (d) Q_{sp} of nearly degenerate mode pairs as the overlap length L increases. Crossing of the resonant wavelengths occurs in (a) when anticrossing of their Q factors does in (b). Roman numerals in (b) mark the first ten local maximums of the Q factors. In the shaded region in (b), the Q factor is larger than 10 000. Modulation behavior of the locally high Q factors is clearly visible in (b). The same modulation behavior is reproduced for the mode chirality in (c). The inset in (c) gives the angular momentum distribution $|\alpha_m|^2$ for two successive local maximums of the Q factors, showing that the CCW traveling-wave component is dominant for resonant modes in the rolled-up microcavity. The nearly degenerate mode pairs could be resolved in experiments if $Q_{sp} > 1$, as shown in the shaded region in (d).

by using EPs [41,42]. Unfortunately, there is no report on the mode structure (e.g., the nonorthogonality and chirality) in rolled-up microcavities, although they have a well-defined structural chirality. One of the main findings of this work is to show that resonant modes with a high Q factor in a rolled-up microcavity have a high mode chirality.

To investigate the chirality of a nearly degenerate pair of modes in rolled-up microcavities, we need to know the CW and CCW components in the angular momentum representation [40]. To this end, we expand the wave function by the cylindrical harmonics, $\psi(\rho, \phi) = \sum_{m=-\infty}^{\infty} \alpha_m J_m(nk\rho) \exp(im\phi)$, where J_m is the m th-order Bessel function of the first kind, $k = \omega/c$ is the wave number, and negative (positive) values of the angular momentum index m correspond to the CW (CCW) traveling-wave components. It is noted that in the position representation, m is a positive value, and the resonant modes take the form of a standing wave with a $\cos(m\phi)$ or $\sin(m\phi)$ dependence. Now, we can define the mode (spatial) chirality [40] as

$$\alpha = 1 - \frac{\min(\sum_{m=-\infty}^{-1} |\alpha_m|^2, \sum_{m=1}^{\infty} |\alpha_m|^2)}{\max(\sum_{m=-\infty}^{-1} |\alpha_m|^2, \sum_{m=1}^{\infty} |\alpha_m|^2)}, \quad (3)$$

and the results are shown in Fig. 2(c).

An interesting behavior is noted in Figs. 2(a) and 2(b), which show that the local maximum of Q factors is obtained when the resonant wavelength splitting of mode pairs is nearly minimized. This behavior in rolled-up microcavities has been observed in previous numerical studies [30]. Moreover, the formation of long-lived modes (i.e., the high Q modes) near avoided resonance crossings (i.e., the minimum resonant wavelength splitting) is a typical feature of open or dissipative systems [25,30]. Therefore, in rolled-up microcavities the locally increased Q factor can be attributed to the reduction of external decay channels introduced by the local structure singularities (i.e., inner and outer notches) through destructive interference [43]. However, these locally high Q factors are very sensitive to the overlap length L , so they are less meaningful from an experimental point of view. Resonant modes with a high Q factor in a wide range of parameter space are thus required.

Such a requirement of high- Q resonant modes in a wide parameter range can be satisfied. As seen in Fig. 2(b), from an overall perspective, a periodical modulation of high Q factors is observed. High Q factors above 10 000 emerge (e.g., peak iv) at a certain overlap length L and reemerge (e.g., peak x) after the local maximum ($Q < 10,000$) appears twice (e.g., peaks vi and viii). High Q factors in the parameter range of the modulation satisfy the requirement since their average value is enhanced by nearly an order of magnitude. Now, one may doubt whether these nearly degenerate mode pairs can be resolved in experiments. To check that out, the mode-splitting quality Q_{sp} is introduced [40,44] as

$$Q_{sp} = \frac{|\operatorname{Re}(\omega_+) - \operatorname{Re}(\omega_-)|}{|\operatorname{Im}(\omega_+) + \operatorname{Im}(\omega_-)|}, \quad (4)$$

and the results are shown in Fig. 2(d). To resolve the mode pairs in experiments, $Q_{sp} > 1$ is needed. Figure 2(d) reveals that mode pairs in the modulation parameter range of high Q factors are rather easily resolved, so they could appear in experiments. In short, a nontrivial behavior of periodical modulation of high Q factors in the rolled-up microcavity is observed, which would benefit the high- Q requirement in experiments.

Moreover, the modulation of the high Q factor is synchronized with the high mode chirality, as seen in Fig. 2(c). This

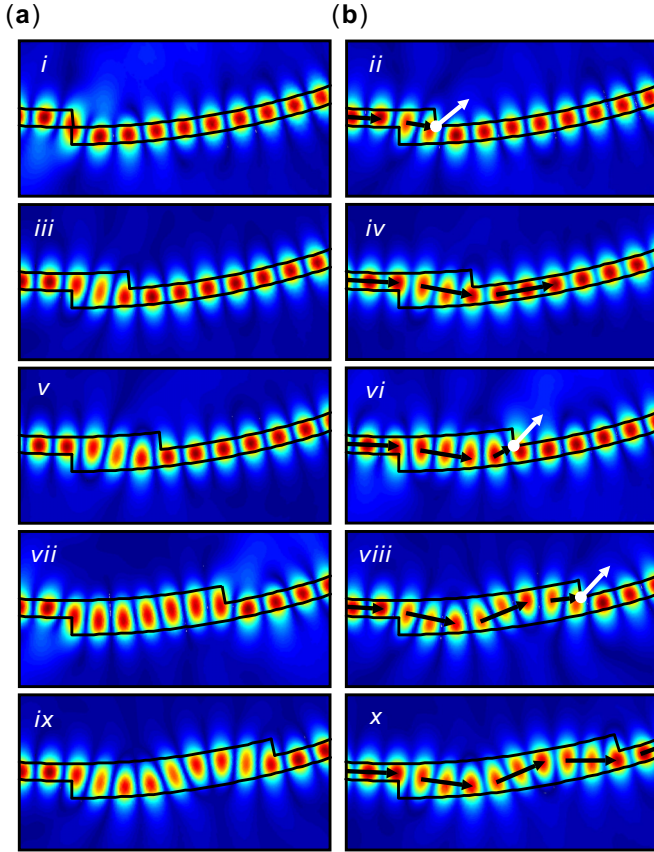


FIG. 3. Electric field intensity $|\psi|^2$ of resonant modes at the first ten local maximums of Q factors marked by Roman numerals in Fig. 2(b). As can be seen, the Roman numerals also indicate approximately the number of antinodes in the overlap area. These modes are classified into two groups in (a) and (b) according to the parity of the number of antinodes in the overlap area. The black arrows show the total internal reflection of resonant light, while the white arrows display its refractive escape.

implies a close relationship between the high Q factor and the high mode chirality, which is the main finding of this work because it cannot be explained by simply considering the destructive interference at the local structure singularities as mentioned above. In what follows, we try to figure out the physics behind the nontrivial modulation behavior of the high Q factor and its close relationship with the high mode chirality in rolled-up microcavities.

The electric field of resonant modes at the first ten local maximums of Q factors is shown in Fig. 3. Based on their similarity to the modulation behavior, these resonant modes can be classified according to the parity of the number of antinodes (the local maximum of electric field) in the overlap area. As seen in Fig. 3, leakage of electric fields at the inner and outer notches is clearly visible, which limits the high Q factors. However, the leakage is less when the overlap length L take values in the parameter range of the modulation, i.e., peaks iii (iv) and ix (x) for the resonant modes with an odd (even) number of antinodes. At these values, the electric field distributes itself to avoid collision at the notches. If we count the number of antinodes in the overlap area, they are 3 (4) and 9

(10). That is to say, high Q factors in the rolled-up microcavity emerge when the number of antinodes in the overlap area takes integers with an interval of 6. In these cases, the electric field of resonant modes can distribute itself continuously from a single wall to another one through the overlap area in a zigzag pattern without meeting the inner and outer notches, so that Q factors of these modes can maintain a high value. In other words, the distribution of electric field in the overlap area presents a qualitative explanation for the periodical modulation of high Q factors in rolled-up microcavities.

Obviously, one cannot clarify the mode chirality directly from the electric field distribution. The Husimi function of resonant modes in rolled-up microcavities is thus investigated, which is an effective tool to show the link between the high mode chirality and the high Q factor of a resonant mode in phase space. It is obtained by the overlap integral of the wave function with a coherent state that represents a minimal-uncertainty wave packet [45]. In the four Husimi functions, the one for the internal emerging wave is widely used and hence is considered here. The internal emerging Husimi function reads [25,45]

$$H^{\text{em}}[\phi, \sin(\chi)] = \frac{nk}{2\pi} \left| \mathcal{F}h_{\psi}[\phi, \sin(\chi)] + \frac{i}{k\mathcal{F}} h_{\partial\psi}[\phi, \sin(\chi)] \right|^2, \quad (5)$$

with a weighting factor $\mathcal{F} = \sqrt{n\cos(\chi)}$, where χ is the angle of internally incident. The function

$$h_g[\phi, \sin(\chi)] = \int_0^{2\pi} d\Phi g(\Phi) \xi[\Phi; \phi, \sin(\chi)] \quad (6)$$

is the overlap integral of the wave function ($g = \psi$) or its normal (radial) derivative ($g = \partial\psi$) on the microcavity's boundary with the minimal-uncertainty wave packet

$$\xi[\Phi; \phi, \sin(\chi)] = (\sigma\pi)^{-\frac{1}{4}} \sum_{l=-\infty}^{\infty} \exp \left[-\frac{(\Phi + 2\pi l - \phi)^2}{2\sigma} - inksin(\chi)(\Phi + 2\pi l) \right], \quad (7)$$

which is centered around $[\phi, \sin(\chi)]$. Here, the parameter σ determines the uncertainty of the wave packet. The Husimi function (5) at the outer boundary of the rolled-up microcavity is shown in Fig. 4. There are two different regions separated by the critical lines $\sin(\chi) = \pm 1/n$. In the region $|\sin(\chi)| > 1/n$, the total internal reflection occurs according to the confined electric field of a resonant mode. Following the convention that the Husimi function with $\sin(\chi) > 0$ ($\sin(\chi) < 0$) stands for the CCW (CW) component, the chirality of the resonant mode can be easily observed. For example, the modes for peaks iii and iv have a high chirality because the Husimi intensity in the CCW region is much greater than that in the CW region, while the mode for peak vi presents a low chirality. The region between the critical lines is called the leaky region, in which refractive escape occurs because χ is smaller than the critical angle $\sin^{-1}(1/n)$ contributed to the far-field of a resonant mode. Obviously, the Q factor of a resonant mode is determined by the Husimi function distributed in the leaky region. For example, the mode for peak vi has more Husimi intensity inside the leaky region, resulting in a low Q factor,

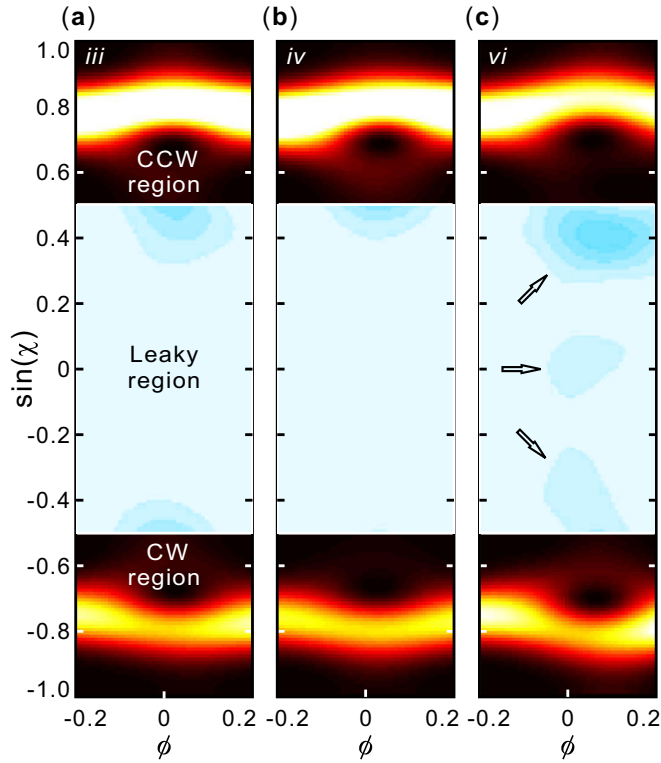


FIG. 4. Internal emerging Husimi function at the outer boundary of the rolled-up microcavity for peaks (a) iii, (b) iv, and (c) vi in Fig. 2(b). A different color map is applied for the leaky region bounded by the critical lines $\sin(\chi) = \pm 1/n$. Black arrows in (c) are guides to the eye.

while the modes for peaks iii and iv have a high Q factor. Therefore, the relationship between the high mode chirality and the high Q factor of a resonant mode is distinguished by simultaneously inspecting the Husimi function distributed in the two regions. For example, the modes for peaks iii and iv have the Husimi function distributed almost in the CCW region, so they have a high mode chirality with a high Q factor. In conclusion, the main finding of this work that high Q factors are due to the high mode chirality of resonant modes in rolled-up microcavities is further evident and directly visualized in phase space via the Husimi function.

IV. THE HAMILTONIAN

In order to clarify the modulation of high Q factors and its close relationship with the high mode chirality in rolled-up microcavities, a two-mode non-Hermitian Hamiltonian is introduced in this section. It is based on the Hamiltonian for two-particle-microdisk systems derived in Ref. [40] owing to the obvious fact that the inner and outer notches in rolled-up microcavities play a role similar to that of the two particles in two-particle-microdisk systems. The Hamiltonian for two-particle-microdisk systems neglected any interaction between the two particles because interactions take place across the microdisk and are generally weak [40], as shown in the left panel of Fig. 5(a). However, as seen from the right panel of Fig. 5(a), interactions between the inner and outer notches of the rolled-up microcavity through its subwavelength-thin wall

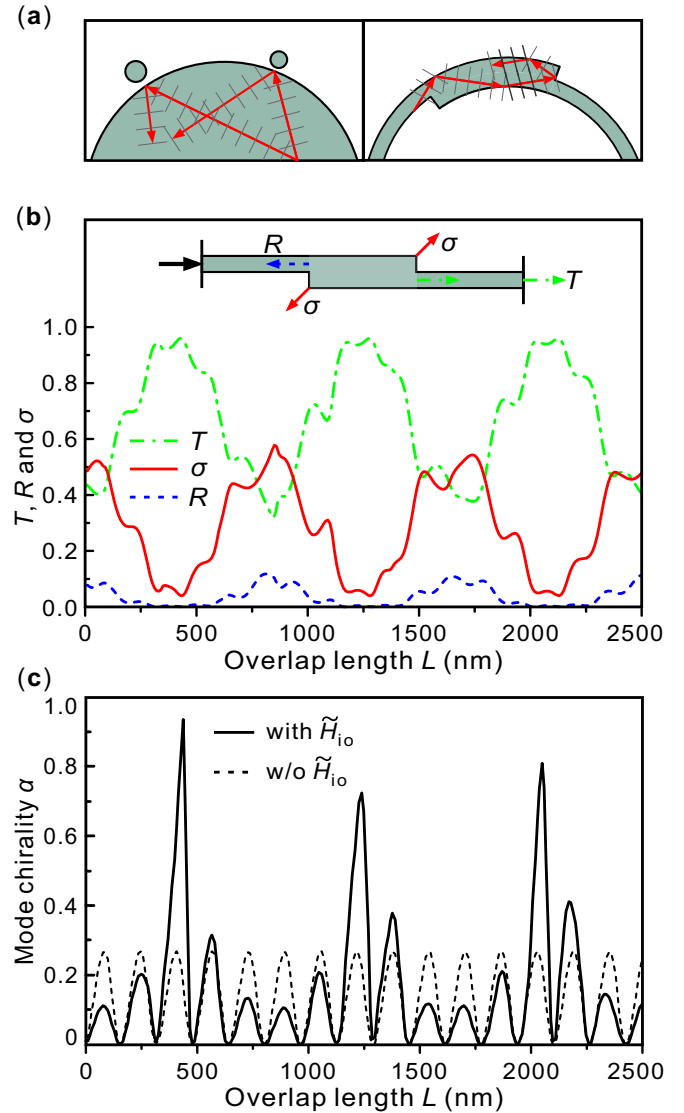


FIG. 5. (a) Left (right): schematic of interactions between two particles (inner and outer notches) via scattered waves propagating across the solid core of two-particle-microdisk systems (through the subwavelength-thin wall of rolled-up microcavities). (b) Scattering of a waveguide mode at the overlap segment formed by two identical waveguides in an add-drop-like configuration. (c) Evolution of mode chirality as a function of the overlap length L calculated with and without considering interactions between notches.

are very strong, so they have to be taken into account in the Hamiltonian for rolled-up microcavities.

The “unperturbed” rolled-up microcavity is defined as a ring microcavity with a wall thickness of t and an outer radius of $R_{\text{avg}} + t/2$. Within the slowly varying envelope approximation, the two-mode Hamiltonian of the unperturbed system for a given degenerate mode pair with the azimuthal mode index m and the frequency Ω_0 , in the traveling-wave basis [CCW, (1,0); CW, (0,1)], is given by

$$\tilde{H}_0 = \begin{pmatrix} \Omega_0 & 0 \\ 0 & \Omega_0 \end{pmatrix}. \quad (8)$$

The perturbation Hamiltonian caused by the presence of inner and outer notches with $L = 0$ can be written, in the standing-wave basis [even mode, (1,0); odd mode, (0,1)], as

$$H_1 = \begin{pmatrix} 2V_1 & 0 \\ 0 & 2U_1 \end{pmatrix}, \quad (9)$$

where $\text{Re}(2V_1)$ [$\text{Re}(2U_1)$] is the frequency shift of the even (odd) mode and $-\text{Im}(2V_1)$ [$-\text{Im}(2U_1)$] is the increase of its decay rate. As a result of this perturbation, the even mode has to distribute itself with even parity relative to the straight line formed by the inner and outer notches [32,46]. Spontaneously, the straight line is antisymmetric with respect to the antinodes of the odd mode. Hence, $|V_1|$ is usually much larger than $|U_1|$. Both U_1 and V_1 are obtained numerically. Now, we need to map the perturbation Hamiltonian H_1 in Eq. (9) from the standing-wave basis to the traveling-wave basis via the transformation matrix $M^\dagger = (1, -i; 1, i)/\sqrt{2}$. The perturbation Hamiltonian in the traveling-wave basis reads

$$\tilde{H}_1 = M^\dagger H_1 M = \begin{pmatrix} V_1 + U_1 & V_1 - U_1 \\ V_1 - U_1 & V_1 + U_1 \end{pmatrix}. \quad (10)$$

The addition of the overlap segment with a length L can be treated as the introduction of N small nanoparticles with the same length $\Delta l = L/N \ll \lambda$ (λ is the wavelength) at a different azimuthal position $\phi = \beta_j$ ($j = 1, 2, \dots, N$ and $\beta_N = \beta$). For the j th nanoparticle, the resulting perturbation Hamiltonian can be obtained in an analogous way, which in the traveling-wave basis reads

$$\tilde{H}_j = \begin{pmatrix} V_2 + U_2 & (V_2 - U_2)e^{-i2m\beta_j} \\ (V_2 - U_2)e^{i2m\beta_j} & V_2 + U_2 \end{pmatrix}. \quad (11)$$

By putting all interactions between the fictitious nanoparticles into an effective interaction Hamiltonian \tilde{H}_{i0} , the perturbation Hamiltonian in the traveling-wave basis reads

$$\tilde{H}_L = \sum_{j=1}^N \tilde{H}_j + \tilde{H}_{i0}. \quad (12)$$

At first, we neglect interactions between notches. In this simple case, $\tilde{H}_{i0} = 0$. The total Hamiltonian without considering interactions between notches takes the form

$$\tilde{H} = \tilde{H}_0 + \tilde{H}_1 + \sum_{j=1}^N \tilde{H}_j = \begin{pmatrix} \Omega & A \\ B & \Omega \end{pmatrix}, \quad (13)$$

with

$$\Omega = \Omega_0 + V_1 + U_1 + N(V_2 + U_2), \quad (14)$$

$$A = V_1 - U_1 + (V_2 - U_2) \frac{e^{i2m\beta} - 1}{e^{i2m\beta/N} - 1} e^{-i2m\beta}, \quad (15)$$

$$B = V_1 - U_1 + (V_2 - U_2) \frac{e^{i2m\beta} - 1}{e^{i2m\beta/N} - 1}. \quad (16)$$

Eigenvalues and (not normalized) eigenvectors of this total Hamiltonian are given by

$$\Omega_{\pm} = \Omega \pm \sqrt{AB}, \quad (17)$$

$$\psi_{\pm} = \begin{pmatrix} \sqrt{A} \\ \pm \sqrt{B} \end{pmatrix}. \quad (18)$$

Therefore, the mode chirality reads

$$\alpha = 1 - \frac{\min(|A|, |B|)}{\max(|A|, |B|)}, \quad (19)$$

and the results are shown in Fig. 5(c).

Off-diagonal elements of the total Hamiltonian (13) describe the backscattering from the CCW to CW component (B) and from the CW to CCW component (A). Generally, $A \neq B^*$, so that the backscattering between CCW and CW components is asymmetrical, leading to the mode chirality, as seen in Fig. 5(c). In the situation with $\beta = \ell\pi/m$, with $\ell \in \mathbb{N}$, i.e., where the inner notch is on every antinode of the even mode, $A = B = V_1 - U_1$, so there is no chiral mode. Apart from this, $A \neq B$, and the biggest difference between $|A|$ and $|B|$ emerges when $\beta = (\ell + 1/2)\pi/m$, i.e., when the inner notch is on every node of the even mode. As a result, there is only one local maximum of mode chirality when the inner notch varies from one antinode to the next. This theoretical result gives the same period of the locally high mode chirality as that observed in the numerical simulations [Fig. 2(c)].

Now, interactions between notches are taken into account to clarify the modulation of these locally high mode chiralities. Because of the inner and outer notches, an overlap segment is formed asymmetrically, connecting the subwavelength-thin wall [see the inset in Fig. 5(b)]. It resembles two identical waveguides coupled through a resonant element in an add-drop configuration [47]. According to the quantum theory of scattering, transport properties of a waveguide mode are modified and dominated by resonances within the resonant element [47–49]. As a result, the Lippmann-Schwinger formalism could be applied to deal with such a resonant scattering process. However, it is difficult to write down a simple and explicit expression of \tilde{H}_{i0} for our asymmetric add-drop-like structure. An approximate treatment is thus proposed here to involve resonances within the overlap segment.

As shown in Fig. 5(b), we numerically calculated the scattering coefficients [i.e., the transmission T , reflection R , and dissipation σ ($\sigma = 1 - T - R$) coefficient] of a propagating wave with frequency Ω_0 from a straight waveguide with a thickness of t to another one through an overlap segment with a length of L . Resonances are clearly visible, and the electric field intensity of these resonant modes has a zigzag pattern without colliding with the notches, similar to that of modes in the modulation parameter range of high Q factors (Fig. 3). Because of these resonances, the perturbation Hamiltonian of the fictitious nanoparticles $\tilde{H}_L = \sum_{j=1}^N \tilde{H}_j$ has to be modified, which is valid only on the condition that all the scattering coefficients are the same as that of $L = 0$ (equivalent to neglecting interactions between notches). Since a resonance is associated with reduced scattering loss, the interaction Hamiltonian \tilde{H}_{i0} is treated as linearly proportional to the noninteraction one $\sum_{j=1}^N \tilde{H}_j$, with the ratio of dissipation coefficients $\sigma(L)/\sigma(0)$ being the proportional coefficient. Based on this approximation, the total Hamiltonian when

considering interactions between notches takes the form

$$\tilde{H} = \tilde{H}_0 + \tilde{H}_1 + \sum_{j=1}^N \tilde{H}_j + C \frac{\sigma(L)}{\sigma(0)} \sum_{j=1}^N \tilde{H}_j, \quad (20)$$

where C is a fitting parameter. Following the same procedures as those from Eqs. (14) to (19), the results for the mode chirality are given in Fig. 5(c). The modulation behavior of locally high mode chirality is clearly visible and agrees with the simulation results, indicating the same physical origin. In conclusion, strong resonant interactions between notches within the overlap area result in the modulation of locally high mode chirality in rolled-up microcavities.

V. CONCLUSION

We have pointed out that the Q factor of resonant modes in rolled-up microcavities is essentially determined by their mode chirality, which results from an asymmetric transition between the CW and CCW traveling-wave components. The modulation behavior of a locally high Q factor (thus high mode

chirality) has been observed, and the origins of strong resonant interactions between the inner and outer notches via scattered waves within the overlap area imply that high Q factors could be possible in rolled-up microcavities. This finding provides an important clue for fabricating high-performance optical microcavities based on rolled-up technology. In addition, the mode chirality of resonant modes in rolled-up microcavities has the same direction as that of their structural chirality, which is in contrast to the two-particle-microdisk systems where the direction of the mode chirality could be alternated. We believe that this deterministic mode chirality will contribute to the information on deformed microcavities with further efforts on this subject.

ACKNOWLEDGMENTS

This work is supported by the Natural Science Foundation of China (Grant No. 51322201), the Specialized Research Fund for the Doctoral Program of Higher Education (Grant No. 20120071110025), and the Science and Technology Commission of Shanghai Municipality (Grant No. 14JC1400200). The authors gratefully acknowledge Z. Tian for fruitful discussions.

-
- [1] K. J. Vahala, *Nature (London)* **424**, 839 (2003).
 - [2] S. M. Spillane, T. J. Kippenberg, K. J. Vahala, K. W. Goh, E. Wilcut, and H. J. Kimble, *Phys. Rev. A* **71**, 013817 (2005).
 - [3] T. Aoki, B. Dayan, E. Wilcut, W. P. Bowen, A. S. Parkins, T. J. Kippenberg, K. J. Vahala, and H. J. Kimble, *Nature (London)* **443**, 671 (2006).
 - [4] D. J. Alton, N. P. Stern, T. Aoki, H. Lee, E. Ostby, K. J. Vahala, and H. J. Kimble, *Nat. Phys.* **7**, 159 (2011).
 - [5] A. M. Armani, R. P. Kulkarni, S. E. Fraser, R. C. Flagan, and K. J. Vahala, *Science* **317**, 783 (2007).
 - [6] J. Zhu, S. K. Ozdemir, Y.-F. Xiao, L. Li, L. He, D.-R. Chen, and L. Yang, *Nat. Photonics* **4**, 46 (2010).
 - [7] L. Shao, X.-F. Jiang, X.-C. Yu, B.-B. Li, W. R. Clements, F. Vollmer, W. Wang, Y.-F. Xiao, and Q. Gong, *Adv. Mater.* **25**, 5616 (2013).
 - [8] M. D. Baaske, M. R. Foreman, and F. Vollmer, *Nat. Nanotechnol.* **9**, 933 (2014).
 - [9] A. Chiasera, Y. Dumeige, P. Féron, M. Ferrari, Y. Jestin, G. Nunzi Conti, S. Pelli, S. Soria, and G. C. Righini, *Laser Photonics Rev.* **4**, 457 (2010).
 - [10] R. Chen, S. Gupta, Y.-C. Huang, Y. Huo, C. W. Rudy, E. Sanchez, Y. Kim, T. I. Kamins, K. C. Saraswat, and J. S. Harris, *Nano Lett.* **14**, 37 (2014).
 - [11] D. K. Armani, T. J. Kippenberg, S. M. Spillane, and K. J. Vahala, *Nature (London)* **421**, 925 (2003).
 - [12] P. Rabiei, W. H. Steier, C. Zhang, and L. R. Dalton, *J. Lightwave Technol.* **20**, 1968 (2002).
 - [13] M. Pöllinger, D. O'Shea, F. Warken, and A. Rauschenbeutel, *Phys. Rev. Lett.* **103**, 053901 (2009).
 - [14] M. Sumetsky, Y. Dulashko, and R. S. Windeler, *Opt. Lett.* **35**, 898 (2010).
 - [15] J. Wang, T. Zhan, G. Huang, P. K. Chu, and Y. Mei, *Laser Photonics Rev.* **8**, 521 (2014).
 - [16] T. Kipp, H. Welsch, C. Strelow, C. Heyn, and D. Heitmann, *Phys. Rev. Lett.* **96**, 077403 (2006).
 - [17] R. Songmuang, A. Rastelli, S. Mendach, and O. G. Schmidt, *Appl. Phys. Lett.* **90**, 091905 (2007).
 - [18] C. Strelow, H. Rehberg, C. M. Schultz, H. Welsch, C. Heyn, D. Heitmann, and T. Kipp, *Phys. Rev. Lett.* **101**, 127403 (2008).
 - [19] Y. Mei, G. Huang, A. A. Solovev, E. B. Ureña, I. Mönch, F. Ding, T. Reindl, R. K. Y. Fu, P. K. Chu, and O. G. Schmidt, *Adv. Mater.* **20**, 4085 (2008).
 - [20] S. Böttner, S. Li, J. Trommer, S. Kiravittaya, and O. G. Schmidt, *Opt. Lett.* **37**, 5136 (2012).
 - [21] V. A. B. Quiñones, L. Ma, S. Li, M. Jorgensen, S. Kiravittaya, and O. G. Schmidt, *Opt. Lett.* **37**, 4284 (2012).
 - [22] J. Wang, T. Zhan, G. Huang, X. Cui, X. Hu, and Y. Mei, *Opt. Express* **20**, 18555 (2012).
 - [23] E. J. Smith, W. Xi, D. Makarov, I. Mönch, S. Harazim, V. A. B. Quiñones, C. K. Schmidt, Y. Mei, S. Sanchez, and O. G. Schmidt, *Lab Chip* **12**, 1917 (2012).
 - [24] L. B. Ma, S. L. Li, V. M. Fomin, M. Hentschel, J. B. Götze, Y. Yin, M. R. Jorgensen, and O. G. Schmidt, *Nat. Commun.* **7**, 10983 (2016).
 - [25] H. Cao and J. Wiersig, *Rev. Mod. Phys.* **87**, 61 (2015).
 - [26] H.-H. Yu, C.-H. Yi, and C.-M. Kim, *Opt. Express* **23**, 11054 (2015).
 - [27] C.-H. Yi, H.-H. Yu, J.-W. Lee, and C.-M. Kim, *Phys. Rev. E* **91**, 042903 (2015).
 - [28] O. G. Schmidt and K. Eberl, *Nature (London)* **410**, 168 (2001).
 - [29] S. H. Schot, *Hist. Math.* **19**, 385 (1992).
 - [30] C. Strelow, C. M. Schultz, H. Rehberg, M. Sauer, H. Welsch, A. Stemmann, C. Heyn, D. Heitmann, and T. Kipp, *Phys. Rev. B* **85**, 155329 (2012).
 - [31] M. Hosoda and T. Shigaki, *Appl. Phys. Lett.* **90**, 181107 (2007).
 - [32] S. Li, L. Ma, S. Böttner, Y. Mei, M. R. Jorgensen, S. Kiravittaya, and O. G. Schmidt, *Phys. Rev. A* **88**, 033833 (2013).

- [33] J. T. Rubin and L. Deych, *Phys. Rev. A* **81**, 053827 (2010).
- [34] A. Mazzei, S. Götzinger, L. de S. Menezes, G. Zumofen, O. Benson, and V. Sandoghdar, *Phys. Rev. Lett.* **99**, 173603 (2007).
- [35] L. Deych, M. Ostrowski, and Y. Yi, *Opt. Lett.* **36**, 3154 (2011).
- [36] Q. Song and Y. L. Kim, *J. Lightwave Technol.* **28**, 2818 (2010).
- [37] T. J. Kippenberg, A. L. Tchebotareva, J. Kalkman, A. Polman, and K. J. Vahala, *Phys. Rev. Lett.* **103**, 027406 (2009).
- [38] T. J. Kippenberg, *Nat. Photonics* **4**, 9 (2010).
- [39] M. R. Foreman, J. D. Swaim, and F. Vollmer, *Adv. Opt. Photonics* **7**, 168 (2015).
- [40] J. Wiersig, *Phys. Rev. A* **84**, 063828 (2011).
- [41] J. Wiersig, *Phys. Rev. Lett.* **112**, 203901 (2014).
- [42] J. Wiersig, *Phys. Rev. A* **93**, 033809 (2016).
- [43] J. Wiersig, *Phys. Rev. Lett.* **97**, 253901 (2006).
- [44] S. K. Özdemir, J. Zhu, L. He, and L. Yang, *Phys. Rev. A* **83**, 033817 (2011).
- [45] M. Hentschel, H. Schomerus, and R. Schubert, *Europhys. Lett.* **62**, 636 (2003).
- [46] J. Zhu, S. K. Özdemir, L. He, and L. Yang, *Opt. Express* **18**, 23535 (2010).
- [47] S. Fan, P. R. Villeneuve, J. D. Joannopoulos, and H. A. Haus, *Phys. Rev. Lett.* **80**, 960 (1998).
- [48] S. Fan, P. R. Villeneuve, J. D. Joannopoulos, M. J. Khan, C. Manolatou, and H. A. Haus, *Phys. Rev. B* **59**, 15882 (1999).
- [49] Y. Xu, Y. Li, R. K. Lee, and A. Yariv, *Phys. Rev. E* **62**, 7389 (2000).